

ORIGINAL ARTICLE

Differential abundance analysis of Procyon and θ Sculptoris: Comparison with abundance patterns of solar-like pairs

Charles R. Cowley¹ | Kutluay Yüce² | Donald J. Bord³¹Department of Astronomy, University of Michigan, Ann Arbor, Michigan²Department of Astronomy and Space Sciences, Faculty of Science, University of Ankara, Ankara, Turkey³Department of Natural Sciences, University of Michigan–Dearborn, Dearborn, Michigan**Correspondence**C. R. Cowley, Department of Astronomy, University of Michigan, Ann Arbor, 1085 S. University, Michigan 48109-1107.
Email: cowley@umich.edu**Abstract**

The precision differential abundance (PDA) technique is applied to the mid-F stars Procyon and θ Scl using spectra from the ESO UVESPOP library. We relate PDA patterns to endogenous processes related to condensation or to exogenous processes connected to Galactic chemical evolution. We employ one-dimensional LTE models, but emphasize the use of weaker lines (≤ 20 mÅ) that are typically used in such studies. We compare our results with PDAs of solar-type stars. Abundances and PDAs are determined for 28 elements: C, N, O, Na, Mg, Al, Si, S, Ca, Sc, Ti, V, Cr, Mn, Fe, Co, Ni, Cu, Zn, Y, Zr, Ba, La, Ce, Nd, Sm, Eu, and Gd. A plot of PDAs (θ Scl minus Procyon) versus Z shows a highly significant correlation. Moreover, local substructure of the plot for the elements Ca-Zn and neutron-addition elements is similar to that which can be found for solar twins. Our PDA versus Z plot structural shows similarity to plots that can be made from the extensive work of Bedell et al. (2018). That PDA structure and substructure is clearly a function of age.

KEYWORDstars: abundances — stars: solar-type — stars: individual: Procyon — stars: individual: θ Scl

1 | INTRODUCTION

Aller (1963) discussed the differential abundance method used by mid-20th century astronomers. In it, one characterized stellar atmospheres by single, mean values of temperature and pressure. The method allowed one to avoid the use of gf -values which were often highly uncertain. This technique has been revised and updated in connection with analyses of solar twins (Meléndez et al. 2009; Nissen & Gustafsson 2018). In the modern technique, one determines basic stellar parameters and abundances from individual lines in the standard way (Gray 2005), using model atmospheres, equivalent widths, and/or spectral synthesis. Differential abundances are then calculated from corresponding line pairs in the twin stars.

A primary advantage of the historical work, near independence from gf -values, is retained. The stars are chosen to have identical or nearly identical spectral types, and presumably closely comparable structures and abundances—to be “twins.” The precision of the method has revealed significant differences which may arise as a result of star formation and Galactic chemical evolution (GCE) (Bedell et al. 2018, henceforth BD18).

2 | THE STARS AND THEIR SPECTRA

Ramírez et al. (2014), henceforth RAM14 carried out an extensive study of mid and late F-star pairs. They noted

that the thinness of the F-star convection zones relative to those of the well-explored solar twins would make it easier to detect abundance anomalies due to, for example, planet formation. Rather than making comparisons with the Sun, they defined standard stars from within their sample.

In the current work, we choose to compare two similar mid-F stars, slightly hotter than those of the RAM14 sample. Procyon (HD 61421) is a well-studied binary, consisting of an F5 IV-V and a white dwarf. Its composition is generally considered “indistinguishable from solar” (Liebert et al. 2013). The star, θ Scl (HD 739), is a single-lined binary (Fuhrmann et al. 2017; Fuhrmann & Chini 2012). Its spectral type is F5 V. Contributions from the companions of either star are neglected in this study, although Procyon could be affected by pollution from its companion.

Numerous studies have given abundances for Procyon (Liebert et al. 2013). Selective abundances for θ Scl are given by Fuhrmann et al. (2017) and Battistini & Bensby (2015). The former work is not differential, while latter compares F-stars with the Sun and therefore is distinct from twin studies, which usually involve stars with effective temperatures differing by some 100 K or less.

Procyon and θ Scl are in the ESO UVESPOP library (Bagnulo et al. 2003) which provides the high-quality spectra suitable to apply the differential-twin abundance method in the F-star domain. The spectra are of comparable quality to those used to analyze solar twins (S/N 300–700, RP 80,000).

3 | SELECTION AND MEASUREMENT OF THE LINE SPECTRA

Lines were chosen from lists from Bedell et al. (2014) and Nissen (2015), but largely from the Procyon identification list published on Cowley’s web site.¹ We selected lines with no obvious blends for which the measured and Ritz wavelengths were $\leq 0.03 \text{ \AA}$ apart. Emphasis was given to weak ($\leq 20 \text{ m\AA}$) lines (Section 4). Each line was then synthesized to discern the contribution of possible blends. The decision to use a particular line was aided by a synthesis with most of the broadening turned off, for example, no turbulent or instrumental broadening. Additional useful information came from a synthesis with the contribution from the line in question turned off.

We chose to measure equivalent widths with the automatic routine automatic routine for line equivalent widths and spectra (ARES) (Sousa et al. 2015). The code was downloaded from S. G. Sousa’s web site² and installed

TABLE 1 Adopted weak Fe I and Fe II lines

Fe I			Fe II		
$\lambda(\text{\AA})$	$\log(gf)$	Desc.	$\lambda(\text{\AA})$	$\log(gf)$	Desc.
4808.148	−2.668	Sol	4720.139	−4.570	Sol
5295.312	−1.557	Sol	4833.192	−4.621	Sol
5386.333	−1.730	Sol	4953.980	−2.680	Sol
5441.339	−1.588	Sol	5000.730	−4.733	Sol
5491.832	−2.188	C+	5161.175	−4.203	Sol
5696.089	−1.720	C+	5427.816	−1.545	Sol
5855.076	−1.478	C+	5525.117	−3.970	C
6226.734	−2.098	Sol	5591.360	−4.527	Sol
6271.278	−2.703	C+	6113.319	−4.078	Sol
6725.356	−2.212	Sol	6179.390	−2.797	Sol
6733.150	−1.456	Sol	6239.357	−4.812	Sol
6837.006	−1.687	B	6248.907	−2.427	Sol
			6446.407	−1.960	V3

under LINUX. Our own measurements, especially those of K.Y., using IRAF’s Gaussian fits, agreed well with those of ARES. We decided that automatic measurements would remove any influence of a personal equation from the results if the input parameters to ARES are the same for both stars.

4 | MODELS AND SOFTWARE

Atlas9 models with solar abundances were used by both C.R.C. and K.Y. Solar abundances are from Asplund et al. (2009) with updates by Scott et al. (2015), and Grevesse et al. (2015). To obtain abundances from an equivalent width, K.Y. used WIDTH9, while C.R.C. fit Voigt profiles (cf. Cowley et al. 2014, and references therein). We used a set of 22 Fe I and 33 Fe II lines. The equivalent widths of these iron lines ranged from 3 to 90 m \AA . The mean difference of our measurements of $\log(W)$, C.R.C.—K.Y., was 0.0031 dex. These lines were used to determine the microturbulent velocity and to ensure that the abundances were independent of excitation potential.

The standard method of deriving the microturbulence is to require that the stronger lines agree in abundance with the weakest ones. However, this removes virtually all abundance information from the strongest lines. Because of this, we have based our final model parameters on 12 Fe I lines and 13 Fe II lines with equivalent widths $\lesssim 20 \text{ m\AA}$ (Table 1). Our calculations used local thermodynamic equilibrium and 1-dimensional models as is still common in differential analyses (Nissen & Gustafsson 2018).

¹<http://www-personal.umich.edu/~cowley/procyon/wlid.html>

²<http://www.astro.up.pt/~sousasag/ares/>

In order to choose values of T_{eff} and $\log(g)$ for abundance calculations, four or five models were calculated, based on initial estimates from the literature and spectral types. Fe I and II abundances (Ab) were calculated for these models. They were assumed to obey a linear relation:

$$Ab = a \cdot T_{\text{eff}} + b \cdot \log(g) + c. \quad (1)$$

The coefficients were determined separately by least squares for the reduced set of Fe I and Fe II lines (Table 1) and then the right-hand sides of Equation (1) were set equal to each other. This gives a linear relation between T_{eff} and $\log(g)$, or a line on a Kiel Diagram (Hunger 1955). This relation is also a function of the lines chosen and their gf -values (Section 4).

To fix our final T_{eff} and $\log(g)$, we used Strömberg (Smalley 2014) and Geneva (Künzli et al. 1997) photometry, synthesis, and comparison of the Balmer-line profiles, as well as the requirement that Fe I and Fe II yield the same abundance. Our adopted model for Procyon has $T_{\text{eff}} = 6,550$ K and $\log(g) = 3.9$, with $v \cdot \sin(i) = 3.0$ km/s and a microturbulence of 2.0 km/s. For θ Scl, these values were 6,525 K, 4.3, 3.0 km/s, and 1.7 km/s. A possible contribution from macroturbulence is included in our values of $v \cdot \sin(i)$, which were found by spectrum synthesis. These figures are in agreement with values in the literature (Allende Prieto et al. 2002; Fuhrmann & Chini 2012). Uncertainties in the models and their effect on our results are discussed in Section 5.

5 | LINES AND TRANSITION PROBABILITIES: ABUNDANCES

5.1 | Iron

The use of very weak lines has advantages and disadvantages. Weak lines cannot be measured as accurately as stronger ones. In our experience, this is true both for lines measured “by eye” as well as those measured by ARES. Additionally, reliable oscillator strengths are more difficult to find for weak features (see below). On the other hand, curve of growth effects (e.g., microturbulence and hyperfine structure) are reduced by the use of weak lines. In Cowley & Yüce (2019), we found that for a typical Fe I line with an equivalent width of 15.2 mÅ, the saturation effect weakened the line by 17%. Although with differential methods, oscillator strengths cancel, this is only true for very weak lines and for lines where the saturation effects associated with turbulence and damping are taken precisely into account.

Oscillator strengths with national institute of standards and technology (NIST) (Kramida et al. 2019) ratings of C

or better were available for a few of our weak lines. Results using values from BRASS (Laverick et al. 2019) or VALD3 (V3, Ryabchikova et al. 2015) for the remaining lines led to results with wide scatter. For those lines, we ultimately chose solar gf -values derived in this work from ARES measurements using the Kurucz solar flux atlas (Kurucz et al. 1984). The Fe lines and adopted $\log(gf)$ values are shown in Table 1. The column labeled “Desc” gives the NIST accuracy rating or “sol,” to indicate that solar gf -values were adopted. Of 12, the Fe I lines in Table 1, nine overlap with Bedell et al. (2014). For these lines, the agreement is excellent, especially for five of the lines for which solar values were derived. None of our Fe II lines overlapped with Bedell et al. (2014).

5.2 | Other elements

In order to select lines for analysis, ARES was given a list of all lines from the Procyon identification list, which had a single attribute whose wavelength differed by ≤ 0.03 Å. We then chose lines, with a few exceptions, having equivalent widths ≤ 20 mÅ. Of the 174 lines used for abundances, eight have equivalent widths ≥ 20 mÅ. The largest of these was Eu II with 45.5 mÅ in Procyon. Generally, hyperfine structure was not taken into account for our weak lines, but for this line in Eu II, it was approximately taken into account using the data of VALD3.

The regions near all of these lines were synthesized, as described for the iron lines. While virtually all of the lines had small blends, lines were retained unless the blends were estimated to contribute 10% or more to equivalent widths.

All of the lines judged suitable for analysis in the Procyon spectrum were adopted for θ Scl, provided there was an ARES measurement. In a few cases, lines measured by ARES for Procyon were not measured in θ Scl. Usually such lines were discarded from the analysis, but rarely, the lines were remeasured by C.R.C. Such measurements intercompare very well for weak lines with K.Y.’s IRAF values. The lines in question are: Nd II 5092.77, 5092.81 and Gd II 4316.04.

We consulted the bibliographic reference data of NIST (Kramida et al. 2019) to select the most recently determined oscillator strengths. Where practical, we cite original work rather than compilations (see Column 9 in Table 2).

Derived abundances are given in Table 2. The abundances are for $\log(EI/N_{\text{tot}}) = \log(EI/H) - 0.036$. The Difference column is for (θ Scl minus Procyon). The error of the differences is calculated for the N individual line pairs for each spectrum. Data for individual lines are given in Table 3.

TABLE 2 Individual results

Spec.	N	θ Scl		Procyon		Difference		Ref.
		Ab	Err	Ab	Err	Val.	Err	
C I	7	-3.608	0.087	-3.528	0.052	-0.080	0.041	NIST, Kramida et al. (2019), Laverick et al. (2019)
N I	3	-4.204	0.047	-3.982	0.078	-0.222	0.036	NIST, Kramida et al. (2019)
O I	4	-3.195	0.060	-3.201	0.056	0.006	0.067	NIST, Kramida et al. (2019)
Na I	4	-5.915	0.064	-5.771	0.059	-0.144	0.036	NIST, Kramida et al. (2019)
Mg I	3	-4.557	0.130	-4.563	0.090	0.006	0.055	NIST, Kramida et al. (2019), Ryabchikova et al. (2015)
Al I	2	-5.726	0.160	-5.616	0.134	-0.110	0.026	NIST, Kramida et al. (2019), Ryabchikova et al. (2015), Laverick et al. (2019)
Si I	9	-4.490	0.069	-4.414	0.080	-0.076	0.027	NIST, Kramida et al. (2019), Ryabchikova et al. (2015), Laverick et al. (2019)
S I	3	-4.980	0.013	-4.947	0.022	-0.033	0.017	Zatsarinny & Bartschat (2006)
Ca I	3	-5.820	0.024	-5.909	0.019	0.089	0.036	NIST, Kramida et al. (2019), Ryabchikova et al. (2015)
Sc II	3	-9.107	0.067	-9.051	0.074	-0.056	0.052	NIST, Kramida et al. (2019), Lawler & Dakin (1989)
Ti I	13	-7.176	0.027	-7.155	0.043	-0.021	0.019	NIST, Kramida et al. (2019), Lawler et al. (2013)
Ti II	9	-7.126	0.103	-7.163	0.094	0.037	0.020	NIST, Kramida et al. (2019), Ryabchikova et al. (2015), Wood et al. (2013)
V I	7	-8.297	0.029	-8.227	0.017	-0.070	0.021	NIST, Kramida et al. (2019)
V II	2	-8.368	0.007	-8.395	0.000	0.027	0.007	(Biémont et al. 1989), Brewer et al. (2016)
Cr I	11	-6.567	0.030	-6.576	0.036	0.009	0.015	NIST, Kramida et al. (2019), Ryabchikova et al. (2015), (Sobeck et al. 2007)
Cr II	2	-6.427	0.119	-6.420	0.070	-0.007	0.050	Bouazza et al. (2018)
Mn I	6	-6.732	0.074	-6.724	0.090	-0.008	0.017	NIST, Kramida et al. (2019), Ryabchikova et al. (2015)
Fe I	12	-4.699	0.020	-4.673	0.018	-0.026	0.010	NIST, Kramida et al. (2019), solar gf
Fe II	13	-4.691	0.034	-4.675	0.036	-0.016	0.008	NIST, Kramida et al. (2019), solar gf
Co I	6	-7.068	0.154	-7.026	0.141	-0.042	0.014	NIST, Kramida et al. (2019), Ryabchikova et al. (2015)
Ni I	21	-5.961	0.020	-5.918	0.020	-0.043	0.013	NIST, Kramida et al. (2019), Ruczkowski et al. (2017)
Cu I	2	-8.130	0.019	-8.016	0.022	-0.114	0.004	NIST, Kramida et al. (2019), Ryabchikova et al. (2015)
Zn I	1	-7.453		-7.427		-0.026		NIST, Kramida et al. (2019)
Y II	6	-9.904	0.054	-9.914	0.072	0.010	0.021	NIST, Kramida et al. (2019), Palmeri et al. (2017)
Zr II	2	-9.370	0.040	-9.476	0.016	0.106	0.055	Ljung et al. (2006), Quinet et al. (2015)
Ba II	2	-9.899	0.045	-10.086	0.040	0.187	0.005	NIST, Kramida et al. (2019)
La II	4	-10.993	0.124	-11.207	0.121	0.214	0.008	Lawler et al. (2001)
Ce II	3	-10.402	0.056	-10.510	0.063	0.108	0.075	Lawler et al. (2009)
Nd II	5	-10.457	-0.065	-10.654	0.080	0.188	0.027	Den Hartog et al. (2003)
Sm II	3	-11.071	0.054	-11.226	0.087	0.155	0.035	Lawler et al. (2006)
Eu II	1	-11.521		-11.547		0.026	1,2	Ryabchikova et al. (2015)
Gd II	2	-10.482	0.126	-10.610	0.190	0.127	0.065	Den Hartog et al. (2006)

TABLE 3 Sample data table for individual analyzed lines

Spectrum	λ Å	W_λ mÅ	log (gf)	χ eV	log (EI/N_{tot})
C I	4817.373	8.7	-3.080	7.480	-3.317
C I	5023.841	15.8	-2.210	7.950	-3.531
C I	5551.579	7.0	-1.900	8.640	-3.690
Na I	4497.657	19.0	-1.574	2.100	-5.773
Na I	4751.822	9.6	-2.078	2.100	-5.617
Na I	5148.838	5.6	-2.044	2.100	-5.905

Note: A machine-readable version of the complete table is available at the CDS.

6 | ERRORS

We have listed standard errors in Table 2, which are smaller by \sqrt{N} than standard deviations, which can readily be obtained using Table 2. In general, while standard errors are technically correct, standard deviations often give a more realistic estimate of the uncertainties because statistical analysis does not account for systematic errors. The present differential technique should eliminate many systematic errors, however.

The average standard error of our differential abundances (Column 8 of Table 2) is 0.0294 dex. Overall, we have not reached the level of accuracy, 0.01 dex, of the solar twin studies (Meléndez et al. 2009; Nissen 2015), although for a few species, including Fe I and II, our standard errors are of the order of 0.01 dex.

Uncertainties in the model parameters introduce some error. Cowley & Yüce (2019), see Series 3 slide 3) gave results of a differential analysis for two sets of parameters describing Procyon and θ Scl. One set of results for Fe I and Fe II used the current parameters (T_{eff} , $\log g$), the other used (6,550 K, 3.71) for Procyon and (6,550, 4.0) for θ Scl. The differential abundances for Fe I and Fe II were only 0.011 and 0.004 dex, respectively.

To test the sensitivity of the method to the assumed effective temperature, we retain the parameters T_e and $\log(g)$ for Procyon, and use a temperature 100 K lower for θ Scl: $T_e = 6,425$ K. To ensure equal abundances for Fe I and II, we use $\log(g) = 4.16$. The resulting differences, θ Scl minus Procyon then change from the values of Table 2, to -0.078 for Fe I and -0.063 for Fe II. The change in the differences is a significant 0.06 dex.

NLTE corrections were available for a number of our lines from the website at the Max Planck Institute³ (Bergemann & Nordlander 2014). The differential corrections were generally quite small (≤ 0.01 dex). For Ti I and Cr

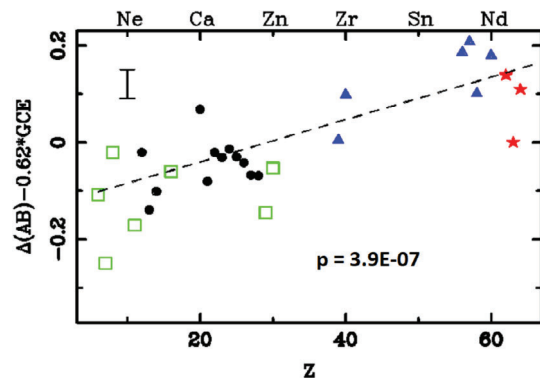


FIGURE 1 Differential logarithmic abundances (θ Scl minus Procyon) versus atomic number Z , with corrections for GCE using an age difference of 0.62 Gyr. The vertical bar has a length of twice the average standard error (Col 8 of Table 2). The dashed line is $\Delta(\text{AB}) - 0.62 \text{ GCE} = 4.38 \times 10^{-3} Z - 0.128$. Green squares are volatile elements C, N, O, Na, S, Cu, and Zn. Blue triangles are elements with a dominant s-process contribution, while red stars have a dominant r-process contribution. GCE, Galactic chemical evolution

I, average corrections were +0.01 and +0.02 dex, respectively, discernable on a graph of our results (Figure 1), but too small to affect the overall conclusions.

A more important source of error arises from the measurement of the equivalent widths. ARES provides an error estimate, ΔW , for each line (Sousa et al. 2015). We used a sample of 194 Fe I lines in Procyon between 3.06 and 20 mÅ. When a line is partially blended or has close neighbors, ARES will model the region, and it gives the number of lines taken into account in determining the equivalent width of an individual line. We took cases where there were no or at most one blending line. Then, the average value of $\Delta W/W$ is 0.0966. We conclude that a typical equivalent width could be $W \pm 0.0966 W$, or roughly $\log(W \pm \Delta W) = \log(W) \pm 0.04$. We take this ΔW to be the standard deviation of the ARES $\log(W)$'s, and compare them with the standard deviations of our logarithmic abundances. The assumption here is that for weak lines, the abundances are proportional to the equivalent widths.

We thus compare this (0.04 dex) standard deviation with estimates of the standard deviation of calculated abundances. We used variances in the differential abundances for 12 Fe I lines and 21 Ni I lines (Table 2), taking them to be representative. Here, the variances are \sqrt{N} times the standard errors in the penultimate column of Table 2. We obtain 0.033 dex for the 12 Fe I lines and 0.063 for the 21 Ni I lines. These are of the same order as the 0.04 dex we derived for the ARES measurements. This is the basis of our belief that the major source of uncertainty in our abundances is the $\log(W)$ measurements. Examination of line-by-line fits and measurements by ARES leads us to conclude that such errors arise as a result of both

³nlte.mpia.de

noise in the spectra and differences in the normalization of the two spectra, and not from the ARES technique itself.

7 | ABUNDANCE TRENDS

When the differential abundances of θ Scl minus Procyon are plotted versus atomic number, a highly significant relation emerges. We use Table 3 of BD18 to see if GCE could account for that correlation. While that table is for the evolution of $[El/Fe]$, the correction to our $[El/H]$ for a relatively short time interval is negligible. We take 0.62 Gyr as a representative age difference based on the 2D linear interpolated values of David & Hillenbrand (2015) who give 1.48 and 2.10 Gyr for the ages of θ Scl and Procyon, respectively. A slightly smaller age difference (0.30 Gyr) results from using their 1D model (most probable) values, but differences in the range of 0 to ~ 4 Gyr based on 68% confidence limits cannot be ruled out.

We subtract from each differential abundance an amount $m\Delta t$, where m is the slope of the BD18 GCE relation for each element, and Δt the difference in the ages of Procyon and θ Scl. The result is shown in Figure 1. For convenience, we refer to the differential abundance as $\Delta(AB)$, rather than $[El/H]$ since the latter is traditionally used for abundance differences with the Sun. Thus, $\Delta(AB) = [El/H]_{\theta Scl} - [El/H]_{Procyon}$.

A linear least-squares fit to the data of Figure 1 is indicated by the dashed line: $\Delta(AB) = 4.38 \times 10^{-3} Z - 0.128$. We shall refer to the coefficient 4.38×10^{-3} as the “overall slope” to avoid confusion with other local slopes to be mentioned below. The fit has a Pearson correlation coefficient of 0.7849 for 28 points. The corresponding probability that the relation arises by chance is $\sim 3.9 \times 10^{-7}$.

The overall slopes of plots like that of Figure 1 for stars of the BD18 sample are well correlated with age (Section 7, Spina et al. 2018), though there is considerable scatter. Only the youngest stars in the BD18 sample (0.5–0.6 Gyr) have slopes as large as 4.38×10^{-3} , and in this case, the age difference of these stars with the Sun is some 4 Gyr. It is unlikely that Figure 1 for our stars, whose probable age difference is less than ~ 1 Gyr, has its slope solely as a result of GCE. By the same token, given the uncertainties of the age estimates and the scatter in the relation between slope and age, we cannot completely exclude some contributions from GCE.

In Figure 2, we compare our differential abundances, $\Delta(AB)$, with the 50% condensation temperature, T_c (Lodders 2003). The small correction for GCE has not been made for this plot. The probability that this plot arises by chance is 0.0028. One can make a case, though not a strong one, for the relevance of temperature-dependent condensation. Similar plots have been made by many authors in

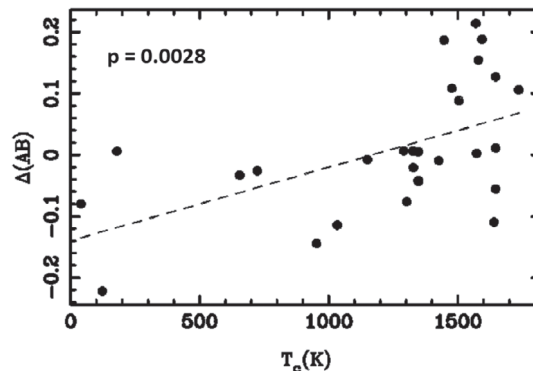


FIGURE 2 Differential abundances versus condensation temperature. The dashed line has the equation $\Delta(AB) = 1.20 \times 10^{-4} T_c - 0.140$

connection with solar twins (Nissen & Gustafsson 2018). Much tighter correlations are shown by Meléndez et al. (2009).

Similar trends with T_c are found in a wide variety of astronomical sources from the interstellar medium (ISM, Jenkins 2003), λ Boo stars (Heiter 2002), Post-AGB stars (Van Winkel 2003), Herbig Ae/Be stars (Folsom et al. 2012), and solar twins (Meléndez Meléndez et al. 2009). The first ionization potential effects (FIP, Laming 2015) observed in the solar and stellar coronae separate elements such as C, N, and O from heavier, iron-group elements. These chemical anomalies cover a wide range of magnitudes, from several dex in the ISM to a few hundredths of a dex in the Sun vs. solar twins. They also occur in a wide variety of astronomical settings. It is not surprising that the observed abundance patterns are variegated.

Ample discussion exists in the literature of possible scenarios that might explain such observations. These range from consequences of terrestrial planet formation to accretion of differentiated interstellar material. We refer to Nissen & Gustafsson (2018, see Section 4), RAM14, and other cited papers for details.

8 | ABUNDANCE PATTERNS IN THE BEDELL SAMPLE

We had expected that the differential abundances of θ Scl versus Procyon to be random, as the stars were so similar in spectral type and population. The structure displayed in Figure 1 led us to examine other differential results.

BD18 published precision differential abundance (PDA) results for 79 solar-type stars. The focus of that and larger studies by Delgado Mena et al. (2019) or Brewer et al. (2016) is primarily on the element to element abundance variations. However, the coverage of Z in the latter studies was not as complete as BD18, so we do not discuss them further here.

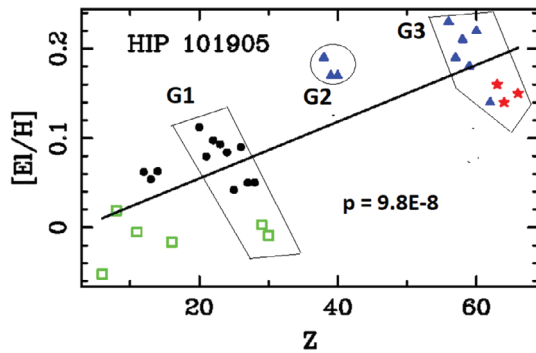


FIGURE 3 Differential abundances for HIP 101905 versus Z showing characteristic trends and groupings of a major portion of the BD18 stars. The age of HIP 101905 is estimated to be 1.2 Gyr. The solid line has the equation: $[E/H] = 3.18 \times 10^{-3} Z - 0.0088$. Symbols are as in Figure 1

Our plots versus Z display the collective behavior of numerous elements. We find a variety of patterns, many of which resemble our Figure 1. Figure 3 is an example of one such plot for 30 elements, carbon through dysprosium. Of BD18's 79-star sample, 35 stars show overall linear fits that are significant at the ≤ 0.01 probability level. The overall slope of those fits correlate well with age. The "local" groups G1 and G3 have significant negative slopes. G1 consists of Ca ($Z = 20$) through Zn ($Z = 30$), of the first long period of the Periodic Table. A straight-line fit with significance ≤ 0.01 can be obtained for the G1 points for about a third of the BD18 sample. G1 remains a coherent configuration even in some stars where the overall slope is no longer well defined, as is typical for many of the older stars. Note that G1 consists of a sequence of elements with decreasing T_c and FIP.

Roughly, a third of BD18's older stars have "V-like" shapes, due to the drop of the G2 group, as shown in Figure 4. Note that G3 has rotated, and now has a positive slope. This positive slope is characteristic of older stars, and contributes to the V-like pattern.

9 | SUMMARY

The technique of PDAs has been applied to the closely similar F-stars Procyon and θ Scl. A plot of abundance differences in the sense θ Scl minus Procyon against atomic number Z shows a highly significant positive slope and a distinct nonrandom pattern. This trend is unlikely to be due solely to GCE. Similar patterns are found among solar-type stars in the survey of BD18, where nearly half of the 79 stars included in that sample display statistically significant overall fits, the (positive) slopes of which are correlated with age. Older stars of the BD18 collection often display markedly different patterns of differential

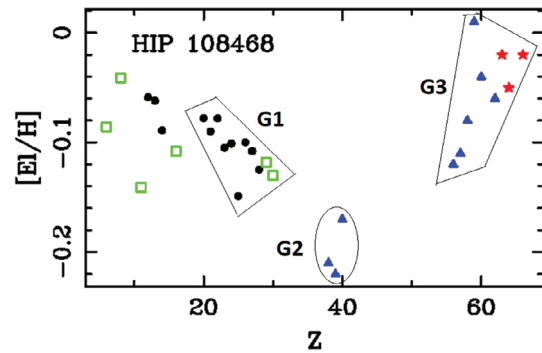


FIGURE 4 Differential abundances for the 7.4 Gyr star HIP 108468 versus Z , illustrating the second major differential abundance pattern of the BD18 stars. Symbols are as in Figure 1

abundance as a function of Z . A full description of the patterns and correlations within the BD18 sample will be presented in a forthcoming paper. Differential abundances for θ Scl and Procyon appear to be only weakly correlated with condensation temperature.

ACKNOWLEDGMENTS

This work made use of the VALD database, operated at Uppsala Universitet, the Institute of Astronomy RAS in Moscow, and the Universität Wien. We acknowledge with thanks the online facilities of NIST and the Belgian Repository of Fundamental Atomic Data and Stellar Spectra. We acknowledge use of data from the UVES Paranal Observatory Project (ESO DDT Program ID 266 D-5655). We thank Megan Bedell and Richard Monier for comments. C.R.C. thanks Pierre North and Barry Smalley for photometric codes. He also thanks his Michigan colleagues and Kohei Hattori for help and advice. We thank the referee for useful comments and suggestions. K.Y. thanks Saul J. Adelman for help and encouragement.

REFERENCES

- Allende Prieto, C., Asplund, M., Garcia López, R. J., & Lambert, D. L. 2002, *ApJ*, 567, 544.
- Aller, L. H. 1963, *Astrophysics: The Atmospheres of the Sun and Stars*, Ronald Press Co. (New York).
- Asplund, M., Grevesse, N., Sauval, J., & Scott, P. 2009, *ARA&A*, 47, 481.
- Bagnulo, S., Jehin, E., Ledoux, R., et al. 2003, *ESO Messenger*, 114, 10.
- Battistini, C., & Bensby, T. 2015, *A&A*, 577, A9.
- Bedell, M., Meléndez, J., Bean, J. L., et al. 2014, *ApJ*, 795, 23.
- Bedell, M., Bean, J. L., Meléndez, J., et al. 2018, *ApJ*, 865, 68 (BD18).
- Bergemann, M., & Nordlander, T. 2014, *Determination of Atmospheric Parameters of B-, A-, F-, and G-Type Stars*, Springer (Cham), 169.
- Biémont, E., Grevesse, N., Faires, L. M., et al. 1989, *A&A*, 209, 391.
- Bouazza, S., Palmeri, P., & Quinet, P. 2018, *At. Data Nucl. Data Tables*, 120, 338.
- Brewer, J. M., Fischer, D. A., Valenti, J. A., et al. 2016, *ApJS*, 225, 32.

- Cowley, C. R. & Yüce, K. 2019. Retrieved from <https://aas234-aas.ipostersessions.com/default.aspx?s=88-0E-2E-9F-EF-B5-F8-77-81-2D-78-25-41-DA-DC-71>
- Cowley, C. R., Hubrig, S., & Przybilla, N. 2014, *MNRAS*, 440, 2457.
- David, T. J., & Hillenbrand, L. A. 2015, *ApJ*, 804, 146.
- Delgado Mena, E., Moya, A., Tsantaki, M., et al. 2019, *A&A*, 624, 78.
- Den Hartog, E. A., Lawler, J. E., Sneden, C., & Cowan, J. J. 2003, *ApJS*, 148, 543.
- Den Hartog, E. A., Lawler, J. E., Sneden, C., & Cowan, J. J. 2006, *ApJS*, 167, 292.
- Folsom, C. P., Bagnulo, S., Wade, G. A., et al. 2012, *MNRAS*, 422, 2072.
- Fuhrmann, K., & Chini, R. 2012, *ApJS*, 203, 30.
- Fuhrmann, K., Chini, R., Kaderhandt, L., & Chen, Z. 2017, *ApJ*, 836, 139.
- Gray, D. F. 2005, *The Observation and Analysis of Stellar Photospheres*, 3rd. ed. University Press (Cambridge).
- Grevesse, N., Scott, P., Asplund, M., & Sauval, A. J. 2015, *A&A*, 573, 27.
- Heiter, U. 2002, *A&A*, 381, 959.
- Hunger, K. 1955, *ZsfAp*, 36, 42.
- Jenkins, E. B. 2003, *Origin and Evolution of the Elements, Carnegie Observatories Astrophysics Series, Vol. 4*, University Press (Cambridge).
- Kramida, A., Ralchenko, YU., Reader, J. et al. 2019. *NIST Atomic Spectra Database (version 5.6.1)*, [Online]. Gaithersburg, Maryland. Retrieved from <http://physics.nist.gov/asd>.
- Künzli, M., North, P., Kurucz, R. L., & Nicolet, B. 1997, *A&AS*, 122, 51.
- Kurucz, R. L., Furenlid, I., Brault, J. & Testerman, L. 1984, Solar Flux Atlas from 296 to 1300nm, NSO Atlas No. 1.
- Laming, J. M. 2015, *LRSP*, 12,2; arXiv:1504.08325.
- Laverick, M., Lobel, A., Royer, P., et al. 2019, *A&A*, 624, 60.
- Lawler, J. E., & Dakin, J. T. 1989, *JOSA*, B6, 1457.
- Lawler, J. E., Bonvallet, G., & Sneden, C. 2001, *ApJ*, 556, 452.
- Lawler, J. E., Den Hartog, E. A., Sneden, C., & Cowan, J. J. 2006, *ApJS*, 162, 227.
- Lawler, J. E., Sneden, C., Cowan, J. J., et al. 2009, *ApJS*, 182, 51.
- Lawler, J. E., Guzman, A., Wood, M. P., et al. 2013, *ApJS*, 205, 11.
- Liebert, J., Fontaine, G., Young, P. A., et al. 2013, *ApJ*, 769, 7.
- Ljung, G., Nilsson, H., Asplund, M., & Johansson, S. 2006, *A&A*, 456, 1181.
- Lodders, K. 2003, *ApJ*, 591, 1220.
- Meléndez, J., Asplund, M., Gustafsson, B., & Yong, D. 2009, *ApJL*, 704, L66.
- Nissen, P. E. 2015, *A&A*, 579, 52.
- Nissen, P. E., & Gustafsson, B. 2018, *A&AR*, 26, 6.
- Palmeri, P., Quinet, P., Lundberg, L., et al. 2017, *MNRAS*, 471, 532.
- Quinet, P., Bouazza, S., & Palmeri, P. 2015, *JQSRT*, 164, 193.
- Ramírez, I., Meléndez, J., & Asplund, M. 2014, *A&A*, 561, 7 (RAM14).
- Ruczkowski, J., Elantkowska, M., & Dembeżyński, J. 2017, *MNRAS*, 464, 1127.
- Ryabchikova, T., Piskunov, N., Kurucz, R. L., et al. 2015, *Phys. Scr.*, 90, 054005.
- Scott, P., Asplund, M., Grevesse, N., Bergemann, M., & Sauval, A. J. 2015, *A&A*, 573, 26.
- Smalley, B. 2014, *Determination of Atmospheric Parameters of B-, A-, F-, and G-Type Stars*, Springer (Cham), 85.
- Sobeck, J. S., Lawler, J. E., & Sneden, C. 2007, *ApJ*, 667, 1267.
- Sousa, S. G., Santos, N. C., Adibekyan, V., et al. 2015, *A&A*, 577, 67.
- Spina, L., Meléndez, J., Karakas, A. I., et al. 2018, *MNRAS*, 474, 2580.
- Van Winkel, H. 2003, *ARAA*, 41, 391.
- Wood, M. P., Lawler, J. E., Sneden, C., & Cowan, J. J. 2013, *ApJS*, 208, 27.
- Zatsarinny, O., & Bartschat, K. 2006, *J. Phys.*, 39B, 2861.

AUTHOR BIOGRAPHY

Charles R. Cowley is professor emeritus of astronomy at the University of Michigan.

How to cite this article: Cowley CR, Yüce K, Bord DJ. Differential abundance analysis of Procyon and θ Sculptoris: Comparison with abundance patterns of solar-like pairs. *Astron. Nachr.* 2020;341:125–132.
<https://doi.org/10.1002/asna.202013694>